

INTRODUCTION

Coronal holes (CH) are large scale structures in the solar corona characterized by lower density and temperature than the surrounding quiet sun as well as by an **open magnetic field configuration**.

- Their appearance depends on the phase of the solar cycle (Mikhailutsa, 1995^[1]; Ikhsanova and Tavatsherna, 2015^[2]; Bilenko and Tavatsherna, 2016^[3])
- **High-speed solar wind streams (HSS)** are emanating from CHs (Krieger, Timothy, and Roelof, 1973^[4]; Nolte et al., 1976^[5]; Cranmer, 2002^[6]) and as a consequence their development is dependent on the evolution of CHs.
- Interaction of HSSs with the ambient slow solar wind can result in the formation of **co-rotating interaction regions (CIR)**; Wilcox, 1968^[7]; Tsurutani et al., 2006^[8]). Together with HSSs, they are the major cause of **recurrent geomagnetic effects** (Verbanac et al., 2011^[9]).

CH PROPERTIES

We find that 6 out of 8 CHs show a **steady change in area**, characterized by a **growing and a decaying phase**. They are categorized as „regular“ types, while the remaining 2 CHs are **outliers** to the steady change in area. Mostly due to the **influence of external sources** (filament eruptions, merging with or splitting into other CHs and connection to polar CHs).

The growing phase is characterized by a generally increasing trend of the area. This phase lasts until an individual maximum is reached after which the area successively decreases.

According to our 6 regular CHs, the mean magnetic field strength shows **no significant correlation with the change in area** (dotted black) (Fig. 1). Also, it doesn't show any special characteristics in different phases of the CH evolution.

Flux tubes (FTs) are small-scale unipolar magnetic structures of CHs. Those with the mean magnetic field strength $>50\text{G}$ govern the **major part of the CH's signed flux** (Hofmeister et al., 2017^[12]). This persists over each individual evolutions. The number of FTs shows high correlation with the CH area and the mean magnetic field strength depends substantially on the strong FTs and the percentage area they cover (Fig. 2). For the mentioned relations there are **no differences regarding the growing and decaying phase of the evolution**. The data points are evenly scattered and contribute equally to the strong correlation we observe.

METHODS AND DATA

- We analyzed a set of **8 long-lived CHs** observed between September 2010 and November 2015, using 193Å Filtergrams (AIA/SDO) and 720s LoS magnetograms (HMI/SDO).
- The identification and extraction of CHs, as well as all of its parameters was done using **CATCH** (Heinemann et al., 2019^[10]), which is an enhanced intensity thresholding method using a gradient modulation at the CH boundary.
- The peak velocity of the HSSs (originating from CHs under study), was manually extracted from the in-situ plasma velocity profile (observed by ACE; Stone et al., 1998^[11]).

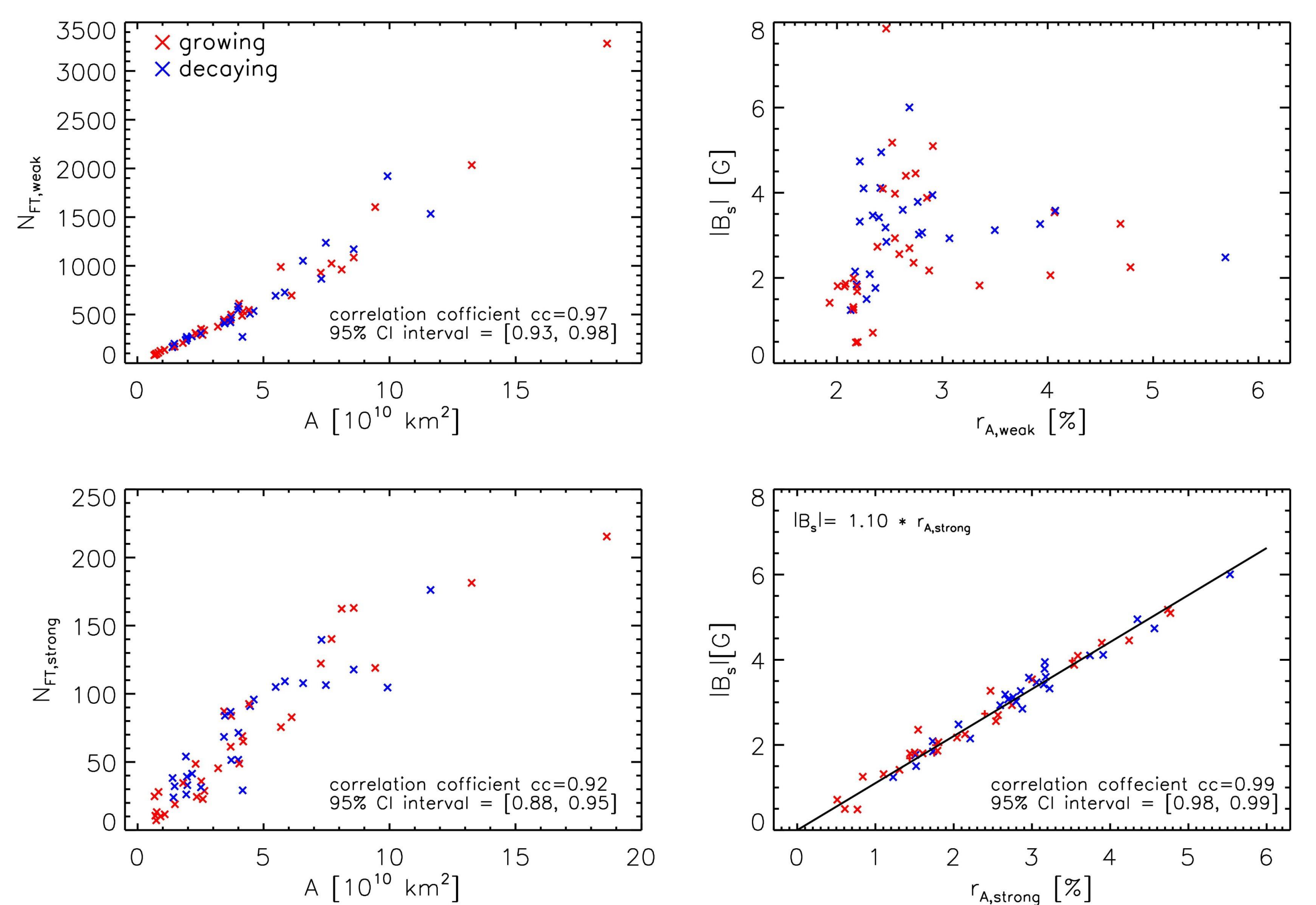


Figure 2. Left panels show scatter plots of the number of FTs (weak FTs – top; strong FTs – bottom) and area of a CH. Right panels show scatter plots of FTs area ratio (weak FTs – top; strong FTs – bottom) and the absolute value of the signed mean magnetic field strength of the CH. Data points are divided between the growing (red) and decaying (blue) part of CH's lifetime. The black line represents the linear fit to the data.

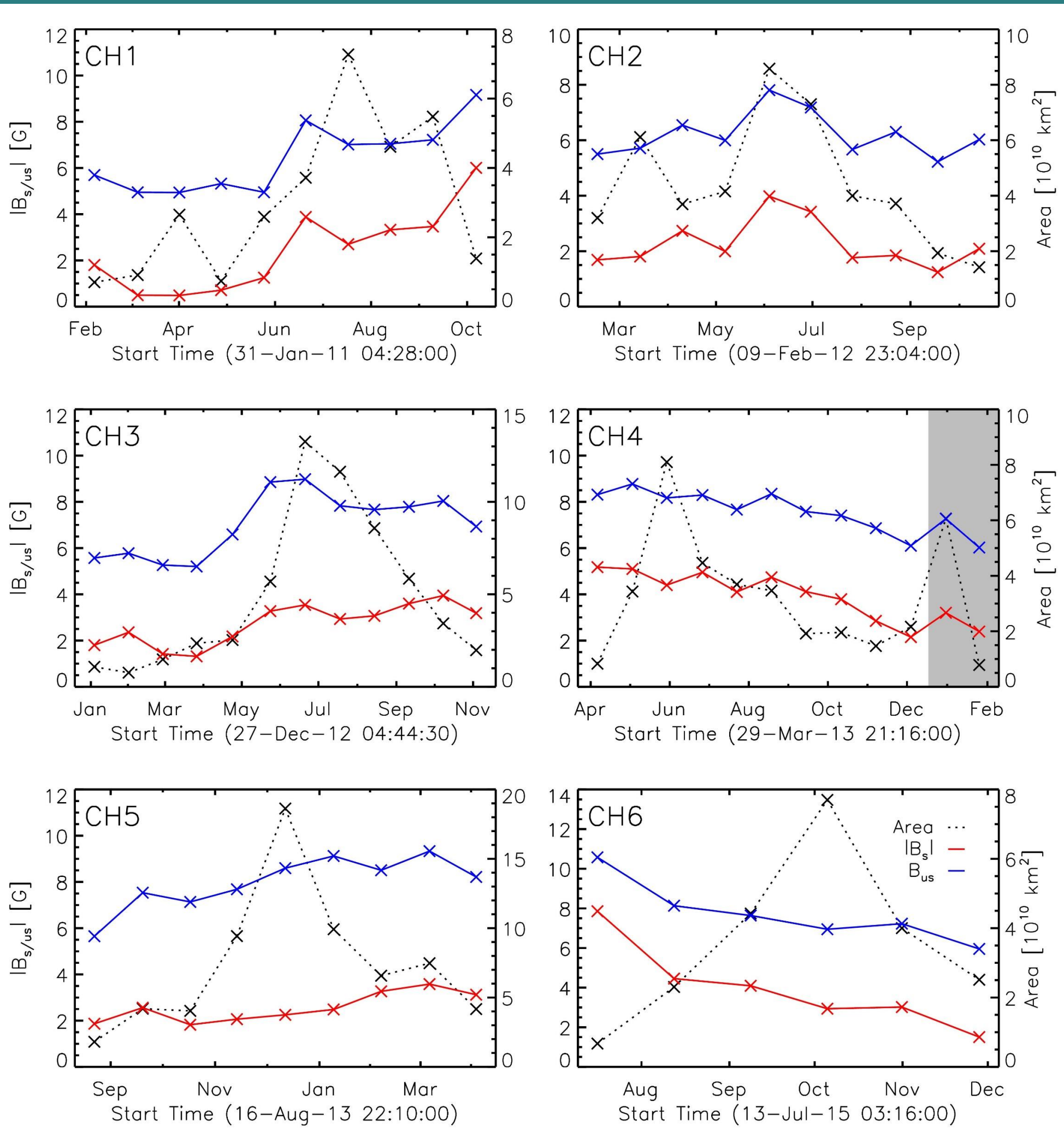
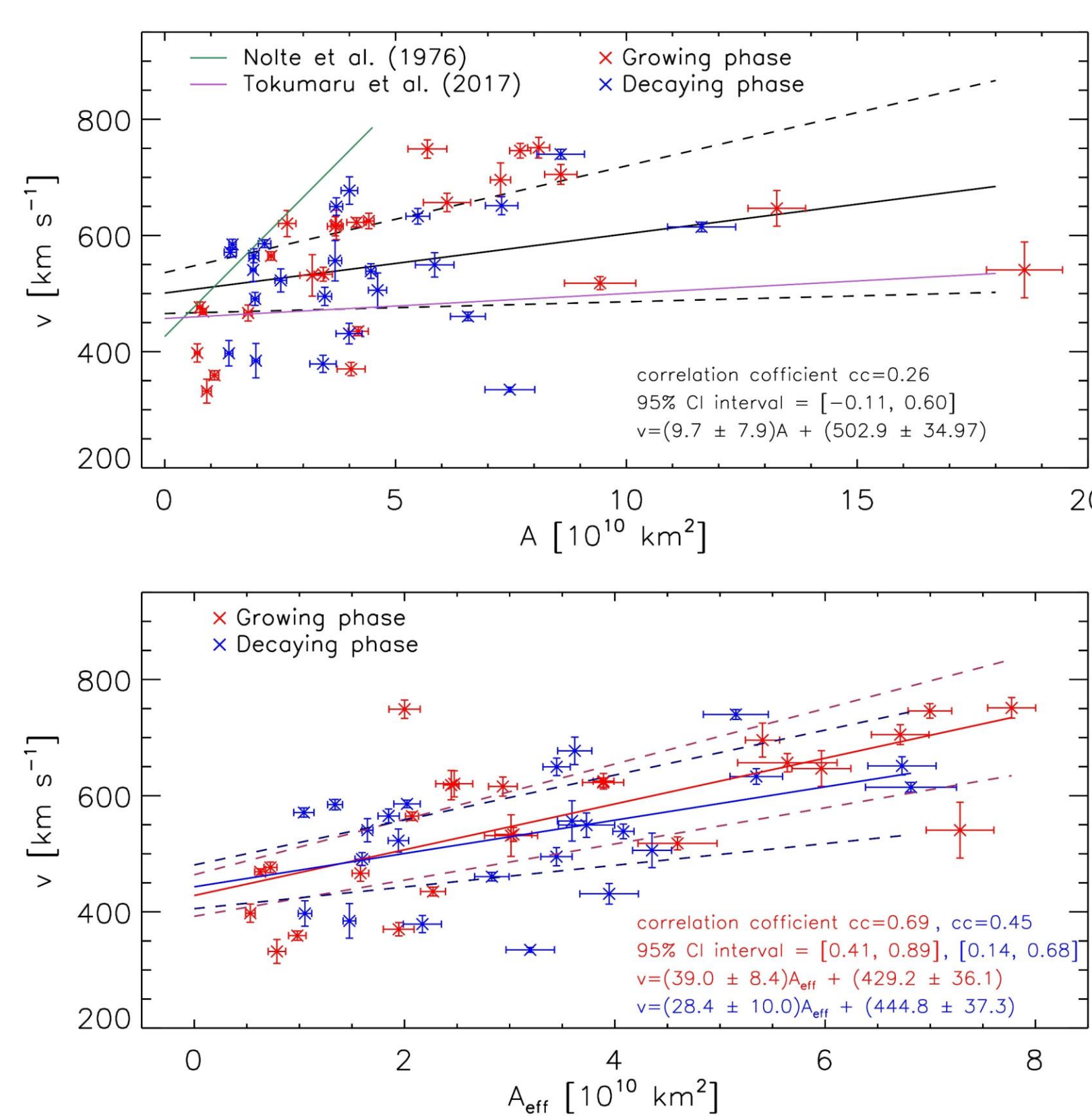


Figure 1. Evolution of signed (red) and unsigned (blue) mean magnetic field strength with CH area (dotted black) for CH1-CH6 (regular types). Absolute values of signed mean magnetic field strength are plotted. The shaded area for CH4 marks the evolution of area influenced by the filament eruption.

SOLAR WIND PROPERTIES



We find that the CH area and the HSS peak speed are well correlated for each individual CH evolution (cc in the range 0.45-0.86). However, when considering the full dataset together, the correlation vanishes (Fig. 3, top). Only after **correcting the CH areas for their co-latitude position** (using an empirical relation from Hofmeister et al., 2018^[13]) the expected relation (e.g. Vrsnak et al., 2007^[14]) is visible (Fig. 3, bottom). We notice an increased correlation with less spread of data points with a **stronger correlation coefficient in the growing (cc=0.69) than in the decaying phase (cc=0.45)**.

Figure 3. Top: HSS peak velocity plotted against CH area. The black solid line represents the linear fit and the dashed lines represent its upper and lower error boundaries. Green and purple lines are two reference fits (Nolte et al., 1976^[4] and Tokumaru et al., 2017^[15], respectively). Growing (red) and decaying (blue) phases of CH evolution are marked in different colors. Bottom: HSS peak velocity plotted against CH area corrected for in-situ co-latitude. The two colored solid lines represent linear fits for each phase and the dashed lines are the corresponding upper and lower error boundary.

CONCLUSION

We found from a sample of 8 well observed CHs, that 6 of them show a **regular pattern of area evolution**.

- Those regular CHs show 2 distinct phases of evolution, **grow and decay**. **Observing changes in the magnetic flux and the HSS over time, we can state that the CH is a rather stable structure in the solar atmosphere during the growing phase and around its maximum.**
- In general, **eruptive events on the Sun** support different processes that cause abrupt changes in the observed CH area. Due to filament eruptions and connections with the polar CH we observe the outliers.
- The **magnetic field** plays an important role in the evolution of CHs and is governed by **strong FTs**. However, because of the unpredictable contribution of FTs to the CH area (either with number or size), **we find no correlation of the evolution of the mean magnetic field strength and CH area.**
- The CH area-HSS bulk speed relation persists during the entire evolution of each individual CH. We attribute the differences between the growing and decaying phase to the **possibility that the dominant driver of the CH evolution differs between the phases**. This might be the cause for the observed differences (e.g., the enhanced scatter in the decaying phase).

REFERENCES

- [1] Mikhailutsa, V. P.: 1995, SoPh, 159, 29
- [2] Ikhsanov, R.N., Tavatsherna, K.S.: 2015, 55, 877
- [3] Bilenko, I. A., Tavatsherna, K. S.: 2016, SoPh, 291, 2329
- [4] Krieger, A.S., Timothy, A.F., Roelof, E.C.: 1973, SoPh, 29, 505
- [5] Nolte, J. T., Krieger, A. S., Timothy, A. F., et al. 1976, SoPh, 46, 303
- [6] Cranmer, S.R.: 2002, SSRv, 101, 229
- [7] Wilcox, J. M.: 1968, SSRv, 8, 258
- [8] Tsurutani, B.T., Gonzalez, W.D., Gonzalez, A.L.C., Guarnieri, F.L., Gopalswamy, N., Grande, M., Kamide, Y., Kasahara, Y., Lu, G., Mann, I., McPherron, R., Soraas, F., Vasyliunas, V.: 2006, RvJGR(Space Physics), 111, A07S01
- [9] Verbanac, G., Vrsnak, B., Zivkovic, S., et al. 2011, A&A, 533, A49
- [10] Heinemann, S. G., Temmer, M., Dissauer, K., Samara, E., Jercic, V., Hofmeister, S. J. & Veronig, A. M.: 2019, in preparation
- [11] Stone, E. C., Frandsen, A. M., Mewaldt, R. A., et al. 1998, SSRv, 86, 1
- [12] Hofmeister, S. J., Veronig, A., Reiss, M. A., et al. 2017, A&A, 635, 268
- [13] Hofmeister, S., Veronig, A., Temmer, M., et al. 2018, JGR, 123
- [14] Vrsnak, B., Temmer, M., & Veronig, A. M. 2007, SoPh, 240, 315
- [15] Tokumaru, M., Satonaka, D., Fujiki, K., Hayashi, K., & Hakamada, K. 2017, SoPh, 292, 41

ACKNOWLEDGEMENTS

The SDO image data and the ACE in-situ data is available by courtesy of NASA and the respective science teams. We also thank the OMNI website at Goddard Space Flight Center, USA for a significant portion of the data used. S.G.H., M.T. and A.M.V. acknowledge funding by the Austrian Space Applications Programme of the Austrian Research Promotion Agency FFG (859729,SWAMI). V. J. acknowledges support from University of Zagreb, Croatia, Erasmus+ program. S.J.H. acknowledges support from the JungforscherInnenfonds der Steiermärkischen Sparkassen.